Chinese Journal of Chemical Engineering 87 (2025) 89–102

Contents lists available at ScienceDirect

Chinese Journal of Chemical Engineering

journal homepage: www.elsevier.com/locate/CJChE

Full Length Article

# Separation of polycyclic aromatic hydrocarbons by solvent screening assisted extractive distillation from FCC diesel

Jun Li , Wanting Yu , Jinsen Gao *

*State Key Laboratory of Heavy Oil Processing, China University of Petroleum (Beijing), Beijing 102249, China*

ARTICLE INFO

*Article history:*
Received 18 June 2025
Received in revised form
15 August 2025
Accepted 2 September 2025
Available online 11 September 2025

*Keywords:*
Polycyclic aromatic hydrocarbons
Extractive distillation
Solvent screening
Quantum chemical calculation

ABSTRACT

The oversupply of diesel in China necessitates efficient separation of polycyclic aromatic hydrocarbons from fluidized catalytic cracking diesel for value-added utilization. However, purification is hindered by alkane and monocyclic aromatic interference. In this work, we propose a solvent-screening strategy for extractive distillation based on molecular polarity and interaction energy analysis. Quantum chemical calculations identified ethylene glycol (aromatic solubility) and *N*,*N*-dimethylformamide (alkane selectivity) as optimal solvents, with weak hydrogen bonds (*e.g.*, O–H···π, C–H···π) governing aromatic interactions. Two process designs were developed: (1) solvent extraction followed by primary extractive distillation (purity >95.0% (mass)) and (2) direct two-stage extractive distillation (purity >92.0% (mass)). This work provides a flexible framework for polycyclic aromatic hydrocarbon separation tailored to market demands while elucidating solvent-solute interactions at the molecular level.


## 1. Introduction

Fluid catalytic cracking (FCC) diesel is a low-quality heavy distillate with a high total aromatic content up to 80% [1,2], of which polycyclic aromatic hydrocarbons (PAHs) account for over 50% [3]. With increasing proportions of heavy oil and residue in petroleum refining processes, FCC diesel production results in elevated resin content, diminished storage stability, and a marked decrease in cetane number [4]. Furthermore, PAHs in commercial diesel are now strictly limited to no more than 7% in compliance with the latest upgraded China VI standards. Consequently, the separation of PAHs from FCC diesel is critical for enhancing diesel quality and enabling value-added utilization of heavy aromatic resources. The production of fine chemicals like rubbers [5], fibers [6], plastics [7], dyes [8], and pharmaceuticals [9] increasingly relies on aromatics, which serve as fundamental organic feedstocks for chemical deep processing. Compared with aromatization reactions derived from hydrocarbons [10], non-destructive physical separation methods directly from fossil resources align more closely with the principles of atomic economy.

Currently, viable techniques for aromatic separation from petroleum and its derived oils include solvent extraction [11,12], extractive distillation [13,14], adsorption [15,16], complexation [17], and membrane separation [18,19]. Among these methods, solvent extraction is widely industrialized due to its low capital investment and mild operating conditions. The emerging green solvents such as ionic liquids and deep eutectic solvents exhibit high selectivity and separation efficiency, but their application to complex mixtures remains largely confined to laboratory-scale studies. In contrast, traditional organic solvents retain irreplaceable process superiority in commercial-scale implementations. In recent years, conventional solvents, including dimethyl sulfoxide (DMSO) [20], sulfolane (SUF) [21], *N*-methylpyrrolidone (NMP) [2], *N*-formylmorpholine (NFM) [22], furfural [23], propylene carbonate [24], and their blends [25], have been employed for aromatic separation in diverse systems.

During the past decades, extensive research has focused on the separation of aromatics and alkanes. Liu *et al.* [20] analyzed the types and strengths of weak interactions in DMSO-decane-aromatic homologue systems, revealing that van der Waals (vdW) forces dominate aromatic-alkane interactions, with electrostatic contributions decreasing and dispersion contributions increasing alongside alkyl chain elongation. Cheng *et al.* [26] systematically investigated the influence of aromatic and alkane structures on extraction performance, demonstrating that distribution coefficients and extraction efficiencies strongly depend

* Corresponding author.
*E-mail address:* jsgao@cup.edu.cn (J. Gao).

https://doi.org/10.1016/j.cjche.2025.09.001

on aromatic structures, while selectivity and aromatic purity are significantly affected by alkane structures. Notably, the disparities in physicochemical property between monocyclic aromatic hydrocarbons (MAHs) and PAHs are far less pronounced than those between alkanes and aromatics, perhaps rendering solvent extraction alone insufficient for efficient separation of aromatics with varying ring numbers. Extractive distillation emerging as a highly feasible approach amplifies relative volatilities through solvent adjustment. Shi *et al.* [27] proposed a fractionation-column chromatography-extractive distillation strategy precisely modulating weak intermolecular interactions to achieve 99.16% (mass) *p*-xylene purity from direct coal liquefaction oil. However, studies on PAHs separation from diesel have predominantly utilized model oils with representative components, with limited reports on direct separation from real FCC diesel. Additionally, MAHs and PAHs exhibit distinct value-added pathways: MAHs are primarily used as premium catalytic cracking feedstocks, whereas PAHs are more suitable for carbon material synthesis *via* polycondensation. Therefore, the isolation of high-purity PAHs from FCC diesel facilitates the high-value utilization of mixed aromatics.

In both solvent extraction and extractive distillation, the solvent serves as the linchpin for MAHs-PAHs separation. Drawing parallels with alkane-aromatic separation, aromatics exhibit a greater propensity to form strong interactions with dearomatization solvents, indicating that the interaction energies of aromatic-solvent complexes are obviously higher than those of alkane-solvent complexes [21]. In other words, aromatics and dearomatization solvents share closer molecular polarity characteristics than alkanes. As a result, the establishment of screening criteria for molecular polarity is necessary to identify potential solvents for efficient dearomatization.

In this work, a universal solvent screening strategy was developed for extractive distillation of PAHs from FCC diesel, integrating quantum chemical calculations with multi-faceted weak interaction analyses. Firstly, multiple molecular polarity parameters have been compared to determine the optimal descriptor, followed by quantifying solvent polarity to identify suitable candidates. Subsequently, representative components undergo electrostatic potential (ESP) analysis to elucidate the most stable solvent-solute complex configurations, with intermolecular interaction energies calculated for each complex. Then we gain deep insights into the primary interaction types and strengths between solvent and solute through quantitative visualization of molecular vdW surfaces, culminating in the identification of the optimal solvent. Moreover, two adaptable processes were designed to accommodate evolving aromatic market demands. The separation performance of individual solvents on real oils was validated to determine main and auxiliary agents, with optimizing operating conditions for both processes. Finally, the universality of this method for PAH separation across diverse FCC diesel sources was systematically evaluated.

**Table 1**
Chemical compositions of the FCC diesels and their extracts.

| Types | FCC-1 | | FCC-2 | | FCC-3 | |
|---|---|---|---|---|---|---|
| Mass components/% | Diesel | Extract | Diesel | Extract | Diesel | Extract |
| Alkane | 14.9 | 5.0 | 23.4 | 4.3 | 26.7 | 4.6 |
| Aromatic | 85.1 | 95.0 | 76.6 | 95.7 | 73.3 | 95.4 |
| Monocyclic aromatic | 22.1 | 22.2 | 41.0 | 41.1 | 19.2 | 17.2 |
| Bicyclic aromatic | 52.5 | 59.1 | 29.3 | 42.5 | 43.8 | 60.8 |
| Tricyclic aromatic | 10.5 | 13.7 | 6.3 | 12.1 | 10.3 | 17.4 |

Note: For convenience, the term 'FCC diesel' in this manuscript always refers to FCC-1 diesel unless otherwise specified.

## 2. Experiment and Calculation

### 2.1. Chemical materials

In this study, DMSO, SUF, NMP, NFM, *N*,*N*-dimethylformamide (DMF), *N*,*N*-dimethylacetamide (DMAC), ethylene glycol (EG), diethylene glycol (DEG), 1,4-butyrolactone (GBL), and ethanolamine (MEA) were provided by Aladdin Biochemical Technology Co., Ltd (Shanghai, China). All chemicals were used as received, and their basic properties are summarized in Table S1. The chemical compositions and physical properties of the three FCC diesels used in this work are listed in Table 1 and Table S2, respectively.

### 2.2. Experimental procedure

#### 2.2.1. Separation process

As illustrated in Fig. 1, two routes for the separation of PAHs from FCC diesel are involved in the process flowchart. The first process involves the extraction of FCC diesel, followed by a primary extractive distillation of the extract to improve the purity and yield of the product. The second process entails conducting extractive distillation directly on the diesel without any pretreatment. However, the presence of a small amount of alkanes in the FCC diesel affects the separation efficiency. Consequently, a secondary extractive distillation of the light fraction obtained from the first-stage extractive distillation is required to enhance the added value of the product. As shown in Fig. S1, the direct distillation and cutting of FCC diesel serves as a blank control.

#### 2.2.2. Extraction experiment

The diagram of the extraction experiment is exhibited in Fig. S2, the experiment comprises the following steps:

a) Specific volumes of diesel and solvent were measured and poured into a round-bottom flask equipped with a stopper. Subsequently, the round-bottom flask was placed in a magnetic stirring water bath, where the desired temperature was set.
b) The mixture was stirred at a specified speed for a certain period of time, then transferred from the flask into a separating funnel and allowed to stand at a constant temperature until the phase interface appeared clearly.
c) After phase splitting, both the extract and the raffinate were washed three times with an equal volume of deionized water. Then, a rotary evaporator was employed to remove the residual water.
d) The masses of the raw material and the samples were recorded separately using an electronic balance, and the mass yields were further calculated based on these recordings. The chemical composition of the samples was analyzed with a gas chromatograph/mass spectrometer.

#### 2.2.3. Extraction distillation experiment

The extractive distillation was performed in a self-made apparatus as shown in Fig. S3, in a typical procedure, the experiment mainly adopted the following steps:

a) Measured volumes of feedstock and solvent were poured into a two-necked round-bottom flask. Then the flask was positioned and fastened within a digitally displayed magnetic stirring heating mantle using a metal clamp.
b) The condensing water was circulated in the condenser, and the system temperature was gradually increased until the temperature was slightly above the boiling point of the

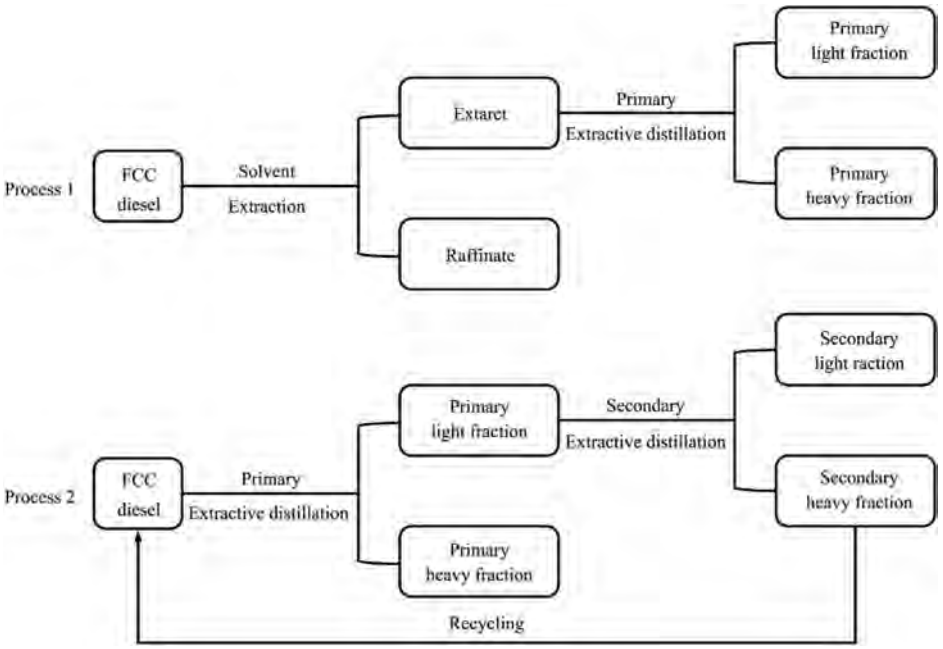


**Fig. 1.** Experimental process flowchart.

solvent used. The system was maintained at this constant temperature for a certain duration until no further components were distilled out, after which the heating power supply was turned off.

c) The flow of condensate was stopped after the distillation column was cooled. The distillate collected in the conical flask consisted of the light fraction and the solvent, while the residue remaining at the bottom of the flask was the heavy fraction, which still contained a small amount of solvent.

d) The fractions were washed three times with an equal volume of deionized water. Then, a rotary evaporator was employed to remove the residual water.

e) The procedures for yield calculation and sample analysis are identical to those employed in the extraction process, and thus will not be reiterated here.

### 2.3. Sample characterizations and evaluation parameters

The composition of samples was analyzed with an Agilent 7890B/5977B gas chromatograph/mass spectrometer, which is equipped with a HP-5MS nonpolar capillary column (30 m × 0.25 mm × 0.25 μm). The oven temperature was initially set at 60 °C and held for 2 min, then it was raised from 60 °C to 300 °C at a rate of 40 °C·min$^{-1}$ and maintained at 300 °C for 10 min. The temperatures of the inlet and flame ionization detector were fixed at 300 °C and 350 °C during the sample analysis, respectively. High-purity helium (99.999%) was used as the carrier gas at a flow rate of 3.0 × 10$^{-5}$ m$^3$·min$^{-1}$. Compound identification was implemented using MSD ChemStation software coupled with the NIST11 library database. The peak area normalization method was conducted to calculate the relative content of the detected compounds in the samples.

Several parameters were defined for the extractive distillation experiments to characterize the separation performance of solvents. The ratio of the mass of fraction to the mass of diesel is defined as the yield.

$$Y_1 = \frac{m_1}{m_F} \tag{1}$$

$$Y_2 = \frac{m_2}{m_F} \tag{2}$$

where $m_1$, $m_2$ and $m_F$ are the masses of light fraction, heavy fraction and feed in extractive distillation, respectively.

In the extractive distillation experiment, the ratio of the mass of MAH in the light fraction to that in the feedstock is defined as the recovery of MAH (denoted as $R_{a1}$). Similarly, the ratio of the mass of PAH in the light fraction to that in the feedstock is defined as the recovery of PAH (denoted as $R_{a2}$). For the heavy fraction, the corresponding ratios for MAHs and PAHs are defined as their respective recoveries (denoted as $R_{A1}$ and $R_{A2}$, respectively).

The mass ratio of MAHs and PAHs in the light fraction from extractive distillation is the distribution coefficient ($D_a$), and similarly, $D_A$ for the heavy fraction, and the ratio of $D_A$ to $D_a$ is the separation factor ($S$).

$$R_{a1} = \frac{m_1 w_{a1}}{m_F w_1} \tag{3}$$

$$R_{a2} = \frac{m_1 w_{a2}}{m_F w_2} \tag{4}$$

$$R_{A1} = \frac{m_2 w_{A1}}{m_F w_1} \tag{5}$$

$$R_{A2} = \frac{m_2 w_{A2}}{m_F w_2} \tag{6}$$

$$D_a = \frac{w_{a2}}{w_{a1}} \tag{7}$$

$$D_A = \frac{w_{A2}}{w_{A1}} \tag{8}$$

$$S=\frac{D_A}{D_a} \tag{9}$$

where $w_{a1}$, $w_{A1}$ and $w_1$ represent the MAH mass contents in the light fraction, heavy fraction and feed, respectively; and $w_{a2}$, $w_{A2}$ and $w_2$ represent those of PAH in the same order.

### 2.4. Quantum chemistry calculation

To gain an insight into the weak interactions between solvents and several model compounds representing the diesel group components during the extractive distillation, the simulation calculations were performed using the Gaussian 09 D.01 package combined with density functional theory. Geometry optimizations and frequency calculations were conducted with the B3LYP functional and 6-311 G(d, p) basis set while the single-point energies were calculated on the optimized structures at the M06-2X/def2-TZVP theory level and minimum structures were confirmed because no imaginary frequency was observed. Moreover, empirical dispersion correction and solvent model based on solute electron density [28] were considered in these calculations. The basis set superposition error was employed to perform corrections on the single-point energy. Furthermore, the possible binding sites between solvent and solute were identified by computing the ESP on vdW surfaces of molecules, using the Multiwfn 3.8 package [29] and the visual molecular dynamics (VMD) program. Additionally, the visual analysis of weak interactions, including atoms in molecules (AIM) topology analysis and reduced density gradient (RDG) analysis were used to judge the interaction type in the system.

## 3. Results and Discussion

### 3.1. Solvent screening

Diverse functional groups in strong polar solvents enable efficient dearomatization by forming robust intermolecular interactions with aromatics. Nevertheless, given the limited polarity difference between PAHs and MAHs, solvent screening is essential to balance selectivity and recovery for efficient separation of alkanes, PAHs and MAHs in diesel extractive distillation.

#### 3.1.1. Screening of the solvent polarity descriptor

In this manuscript, the feasibility of descriptors such as dipole moment, extreme value differences of ESP ($\Delta V$) and the proportion of high ESP regions ($P_A$) on molecular surfaces, and the molecular polarity index (MPI) [30] for quantifying molecular polarity was investigated. The polarity parameters of various solvents, PAHs and MAHs are presented in Table S3. At the same computational level, the calculated dipole moments for strongly polar molecules like EG and apolar molecules such as alkanes (*e.g.*, *n*-hexane) were both found to be 0. This discrepancy may be attributed to the strong dependence of dipole moment on molecular conformation, suggesting that dipole moment as a descriptor could introduce significant errors in assessing molecular polarity. A robust linear correlation ($R^2 > 0.9211$) was observed between $P_A$ and MPI in Fig. 2, indicating that $P_A$ on molecular surfaces is highly linearly correlated with the MPI, and molecules with similar $\Delta V$ values but higher MPIs may exhibit stronger polarity. Furthermore, the calculation results of MPI and $P_A$ were found to be consistent with the polarity of conventional solvents for dearomatization, indicating that quantitative molecular surface analysis can effectively assist in solvent screening.

According to Table S3, MPI values of alkanes range from 10.24 to 13.38 kJ·mol$^{-1}$, whereas those of MAHs range from 23.03 to 35.86 kJ·mol$^{-1}$, and MPI values of PAHs are predominantly greater than 8. Consequently, based on the principle of 'like dissolves like', solvents tend to dissolve compounds with MPI values similar to their own, which aligns with the solubility parameter theory. In other words, solvents with greater molecular polarity are anticipated to exhibit a larger proportion of high ESP areas on their molecular surfaces, thereby enhancing the probability of interaction with PAHs. Using the MPI value as a descriptor, the polarity order of traditional dearomatization solvents is as follows: SUF > DMSO > GBL > DMF > NFM > NMP > EG > DMAC > MEA > DEG.

#### 3.1.2. Intermolecular interaction energy and ESP analysis

The strength of weak interactions can generally be measured by intermolecular interaction energies [31]. As shown in Fig. 3, the interaction energies between aromatic hydrocarbons, alkanes, and solvent molecules, along with their differences, are calculated for further analysis. The calculation results indicate that all alkane molecules exhibit the maximum interaction energy with DMF, whereas all aromatic hydrocarbon molecules show the highest interaction energy with EG. However, SUF was identified as having the highest polarity based on the MPI values discussed above, suggesting that solvent polarity is not the sole determinant of interaction energy strength. The structures and conformations of the two monomeric molecules are also critical factors. It can be found that the interaction energies between aromatics and solvents are generally greater than those between alkanes and solvents. Moreover, PAHs displaying lower structural symmetry exhibit particularly pronounced interaction energies with solvent molecules. This enhanced interaction originates from the extended π-electron conjugation in multi-ring systems, which may facilitate more efficient polarization when exposed to polar solvents. The resulting transient dipole significantly contributes to the overall interaction energy.

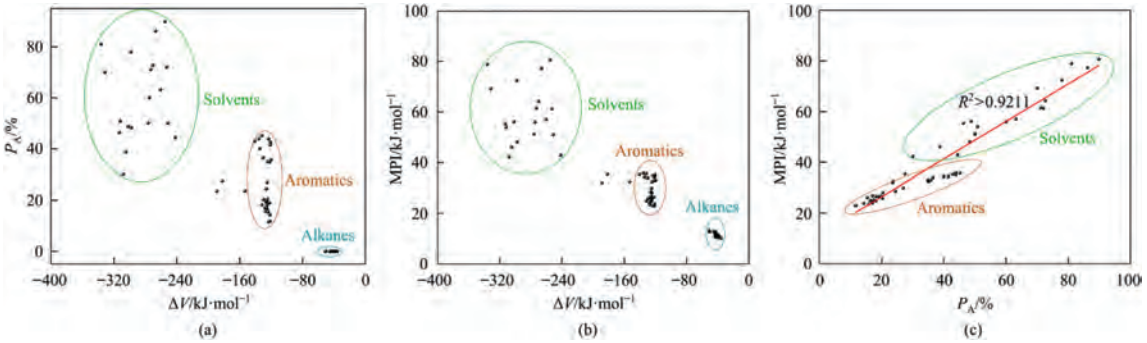


**Fig. 2.** Correlation of three polarity descriptors between solvents, aromactics and alkanes: (a) $\Delta V$ *vs.* $P_A$; (b) $\Delta V$ *vs.* MPI; (c) $P_A$ *vs.* MPI.

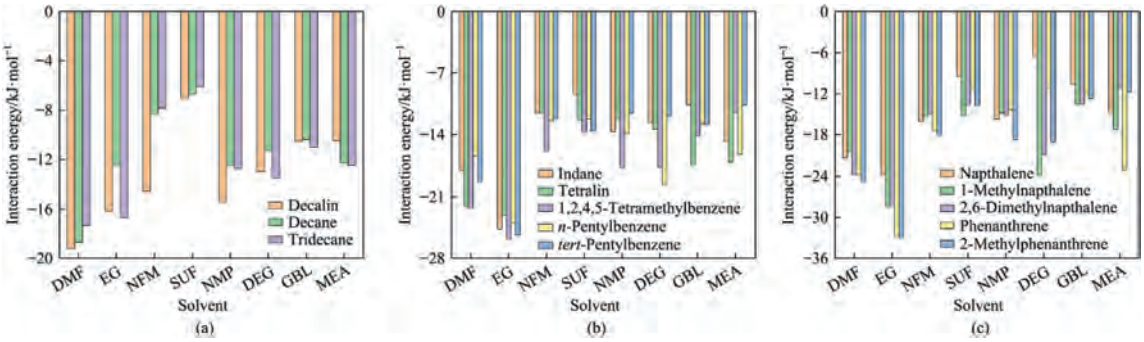


**Fig. 3.** Interaction energies of solvent-component complexes: (a) solvent-alkane; (b) solvent-MAH; (c) solvent-PAH.

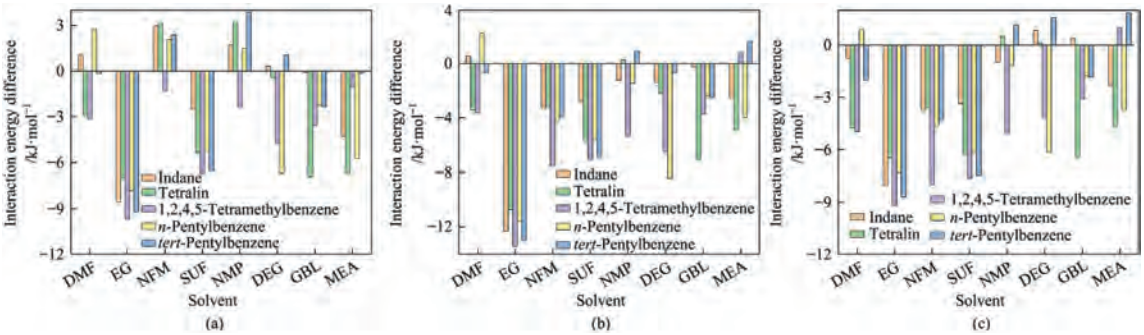


**Fig. 4.** Interaction energy differences between solvent-alkane and solvent-MAH complexes: (a) decalin; (b) decane; (c) tridecane.

The selectivity of solvents towards PAHs and MAHs requires further evaluation based on the extent of differences in interaction energies. A negative $\Delta E$ value, calculated as the difference between solvent-PAH and solvent-MAH interaction energies, indicates preferential solvent selectivity for PAHs over MAHs. Smaller $\Delta E$ values enhance the separation of PAHs from MAHs. It can be observed from Figs. 4–6 that the range of interaction energy differences for alkane-aromatics complexes (−0.11 to −20.54 $kJ \cdot mol^{-1}$) is generally higher than that for MAH-PAH complexes (−0.02 to −12.50 $kJ \cdot mol^{-1}$), and especially when the solvents are DMF, NFM, and NMP, the selectivity of the solvents for all PAHs is greater than that for MAHs. Furthermore, the ranges of interaction energy differences for aromatics with varying ring numbers largely overlap. Consequently, compared to the separation of aromatics from alkanes, it may be challenging to separate PAHs/MAHs in real oil solely through solvent extraction.

ESP analysis was conducted to identify potential binding sites and gain deeper insights into molecular interactions [32,33]. In this study, the ESP distributions of different molecules were visualized using Multiwfn and VMD. As shown in Fig. 7, the blue regions denote the negative ESP values, while the red regions indicate the positive ones. The negative ESP regions of the selected solvent molecules are all concentrated around the positions with heteroatoms. Interestingly, the significant ESP minimum are all concentrated near the oxygen atoms in the solvent molecules, regardless of whether the heteroatoms present are oxygen, nitrogen, or sulfur. In contrast, the ESP maximum are all located near the hydrogen atoms. Notably, the ESP maxima exhibit distinct localization patterns depending on functional groups: in hydroxyl-containing solvents they reside on hydroxyl hydrogens, whereas in other polar solvents (linear or cyclic) they consistently appear on meta-positioned hydrogens relative to oxygen-bonded carbons. As shown in Table S4, the absolute values of the ESP minima for solvent molecules containing hydroxyl groups are significantly smaller than those for solvent molecules containing other polar functional groups. Conversely, the opposite trend exhibited by the

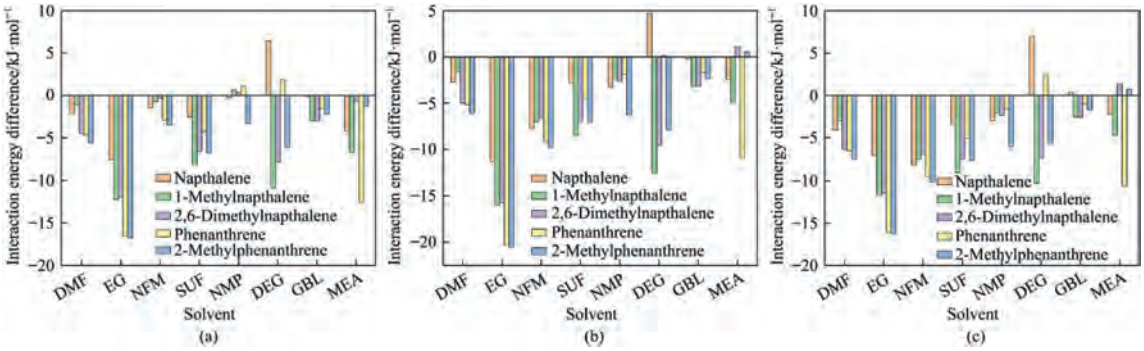


**Fig. 5.** Interaction energy differences between solvent-alkane and solvent-PAH complexes: (a) decalin; (b) decane; (c) tridecane.

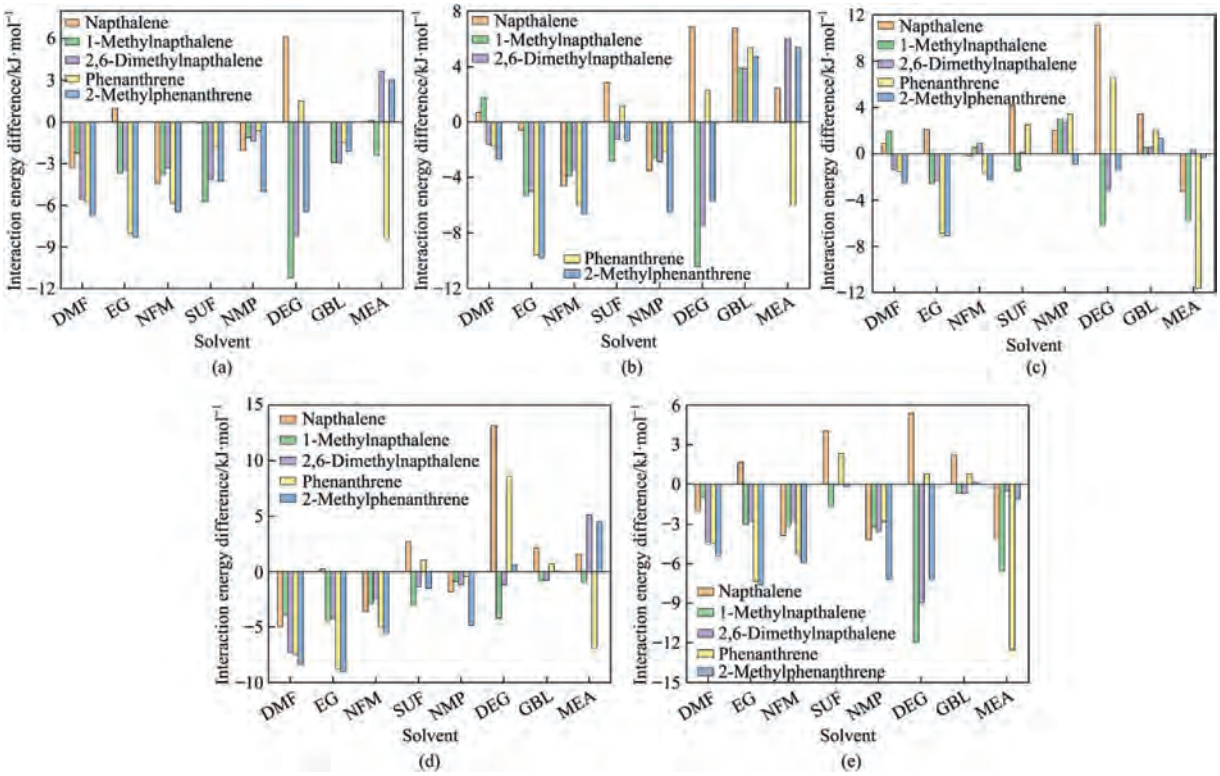


**Fig. 6.** Interaction energy differences between solvent-MAH and solvent-PAH complexes: (a) indane; (b) tetralin; (c) 1,2,4,5-tetramethylbenzene; (d) *n*-pentylbenzene; (e) *tert*-pentylbenzene.

absolute values of the ESP maxima results in a larger $\Delta V$ for solvent molecules with hydroxyl groups as the polar functional group compared to other solvent molecules. It can be inferred that solvent molecules containing hydroxyl groups are more likely to form a "complementary configuration" through the positive ESP regions of the hydroxyl hydrogen atoms and the negative ESP regions of aromatics, thereby minimizing the overall energy of the complex.

### 3.1.3. RDG and AIM analyses

The aforementioned analysis demonstrates that it is feasible to conduct a preliminary screening of target solvents using polarity descriptors, and the predicted results from ESP analysis are fairly consistent with the calculated interaction energies between solvent and solute molecules. However, it remains highly necessary to further investigate the strength and type of intermolecular interactions through weak interaction visualization analysis methods [34] (such as RDG and AIM analysis), which can contribute to an understanding of the nature of solvent-solute interactions.

By taking the representative solvents DMF and EG as examples, the relationship diagrams between RDG and sign($\lambda_2$)$\rho$ for different solvent-solute complexes are plotted in Figs. 8 and 9, respectively. The peaks in the region where sign($\lambda_2$)$\rho$ < 0 in the diagrams indicate the presence of attractive interactions [35], such as

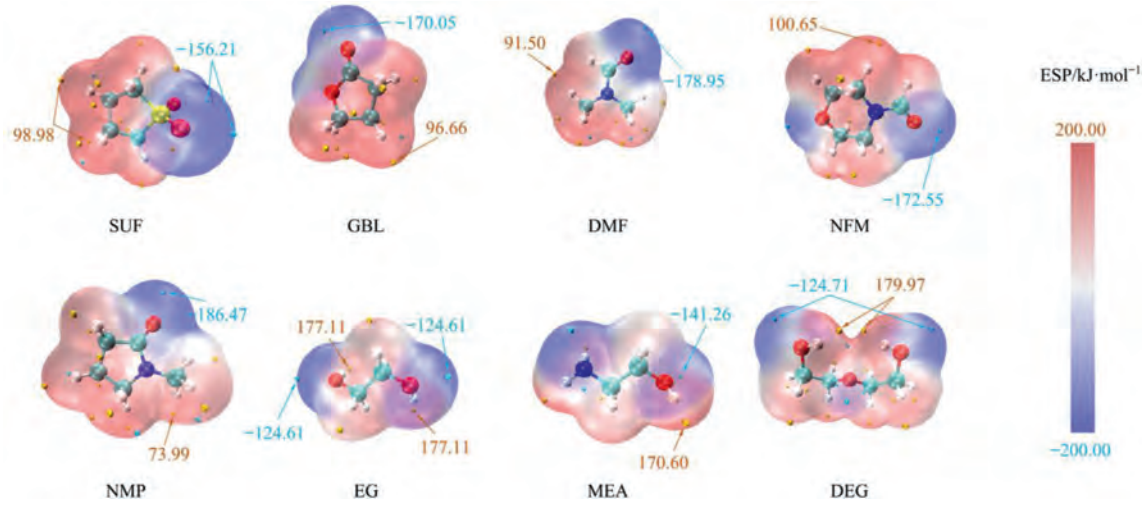


**Fig. 7.** Electrostatic potential diagram of representative solvents.

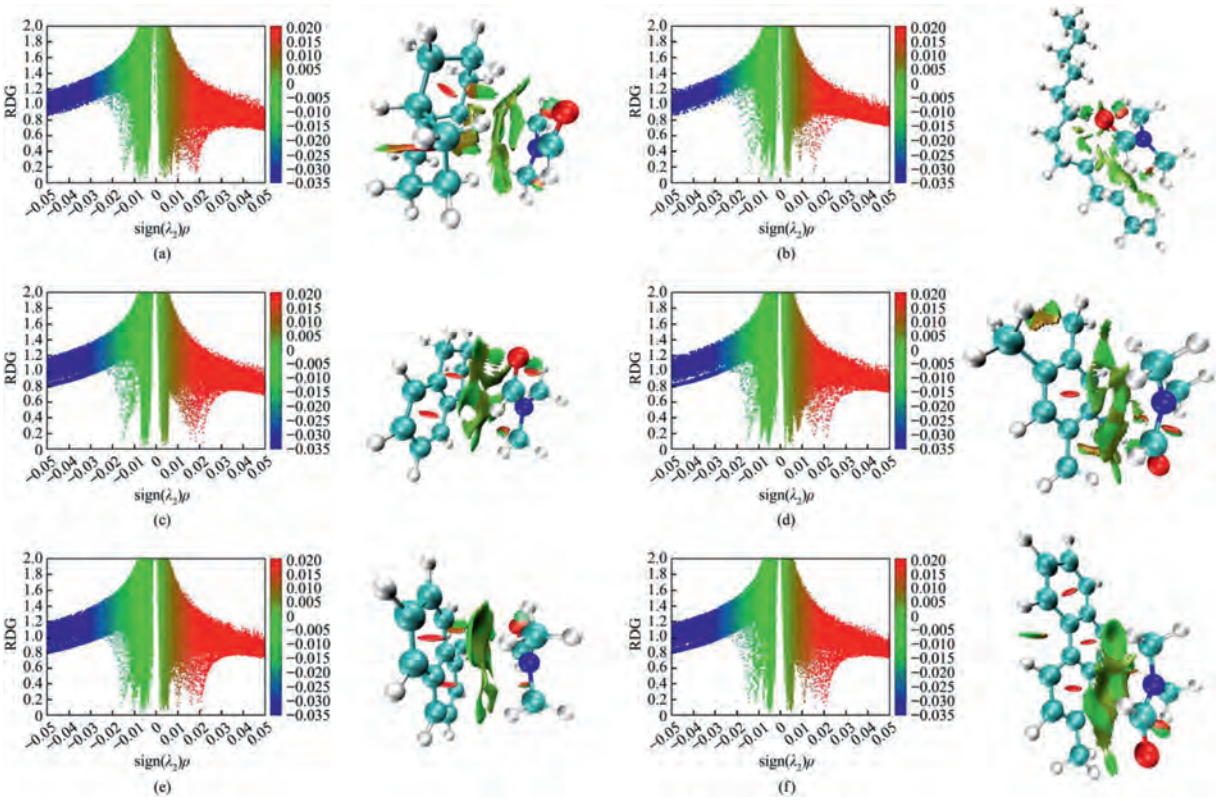


**Fig. 8.** The scatter plot and the gradient isosurfaces of complexes in DMF system: (a) DMF-decalin; (b) DMF-tridecane; (c) DMF-tetralin; (d) DMF-1,2,4,5-tetramethylbenzene; (e) DMF-1-methylnapthalene; (f) DMF-2-methylphenanthrene.

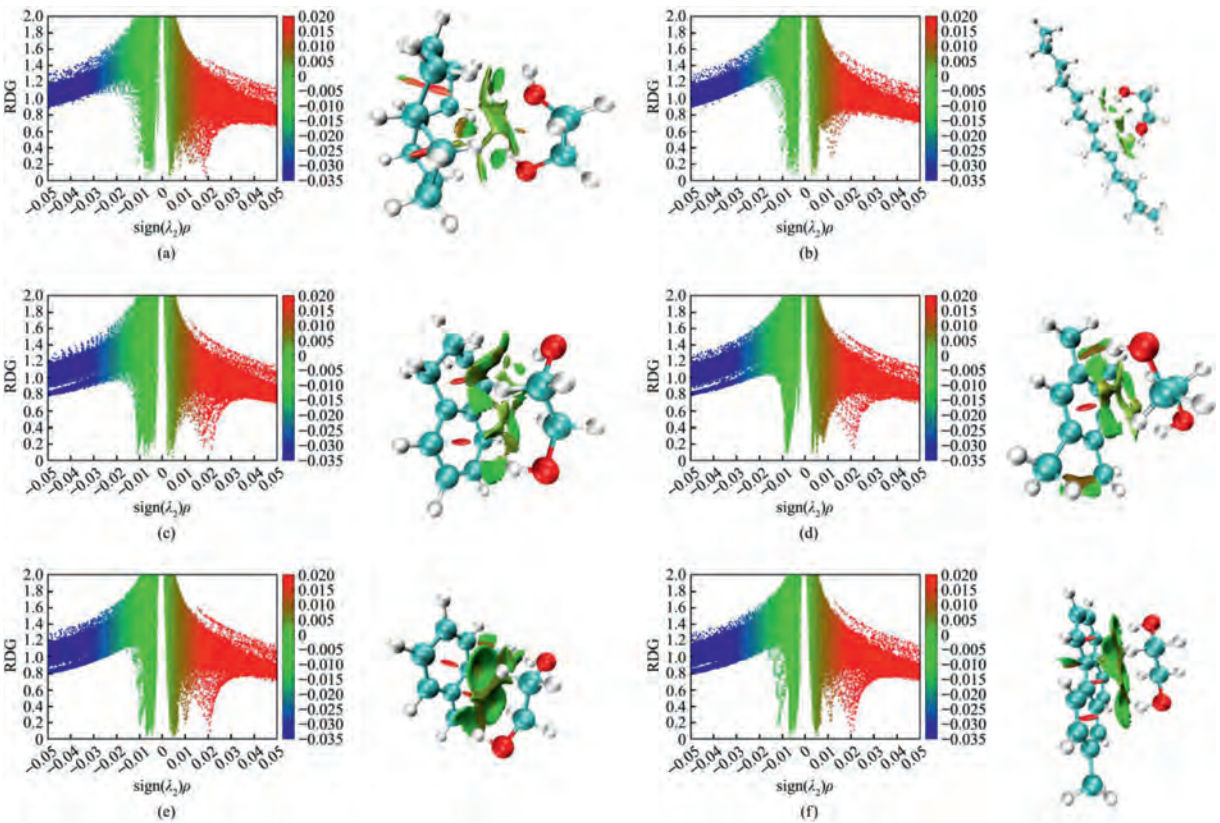


**Fig. 9.** The scatter plot and the gradient isosurfaces of complexes in EG system: (a) EG-decalin; (b) EG-tridecane; (c) EG-tetralin; (d) EG-1,2,4,5-tetramethylbenzene; (e) EG-1-methylnapthalene; (f) EG-2-methylphenanthrene.

hydrogen bonding; the sharp peaks close to zero represent vdW forces; and when the values are large and positive, they correspond to strong steric hindrance effects in the system [36], such as those caused by rings or cages. It can be observed that in the RDG scatter plots of the DMF-solute complexes, there is a sharp peak at around $\text{sign}(\lambda_2)\rho \approx 0.015$ in the red region, implying the existence of a certain degree of steric hindrance effect within the system. Another peak at around $\text{sign}(\lambda_2)\rho \approx -0.015$ may be attributed to the formation of a relatively strong intramolecular C–H···O hydrogen bond during the formation of the DMF-solute complex. This could perhaps explain why DMF, as a straight-chain solvent molecule containing two heteroatom functional groups, exhibits a lower binding energy with aromatics compared to EG. Besides, a sharp peak at around $\text{sign}(\lambda_2)\rho \approx -0.010$ was found in the RDG scatter plots of the EG-aromatic complexes, indicating the presence of interactions between EG and aromatic hydrocarbons that are stronger than typical vdW forces.

In addition, the gradient isosurfaces colored according to the $\text{sign}(\lambda_2)\rho$ values provide rich visualization effects of the interactions, and the types and strengths of the interactions can be identified based on the colors and areas. The blue isosurfaces denote hydrogen bonding interactions, while the green isosurfaces represent vdW force interactions. The predominantly green isosurfaces between all solvents and solutes indicate that vdW forces dominate these systems. In the isosurfaces of all DMF-solute complexes, the N–C═O and C–H groups in the DMF molecule are observed to form a five-membered ring structure. The red isosurface region located at the center of this five-membered ring provides strong evidence supporting our earlier speculation, which is further corroborated by the hydrogen bonding and steric hindrance peaks observed in the RDG scatter plots of these complexes. The calculated interaction energies show that the interaction strength between EG and aromatics increases with the number of aromatic rings, which is positively correlated with the number of hydrogen bonds directed towards the aromatic rings. Moreover, as can be seen from the isosurface diagrams, stable complex configurations are obtained through the formation of unconventional weak hydrogen bonds, such as O–H···π and/or C–H···π, between the hydroxyl and methylene groups of EG and the aromatics.

Furthermore, the AIM analysis was employed to further reveal the weak interactions between solvents and solutes. The parameters related to the chemical bond critical point (BCP) [37] provide quantitative measurements of the nature and strength of the intermolecular interactions, while the bond paths clearly demonstrate the interaction trajectories between two atoms. The presence of BCPs can be characterized and classified by these topological parameters, including the electron density $\rho(r)$, Laplacian

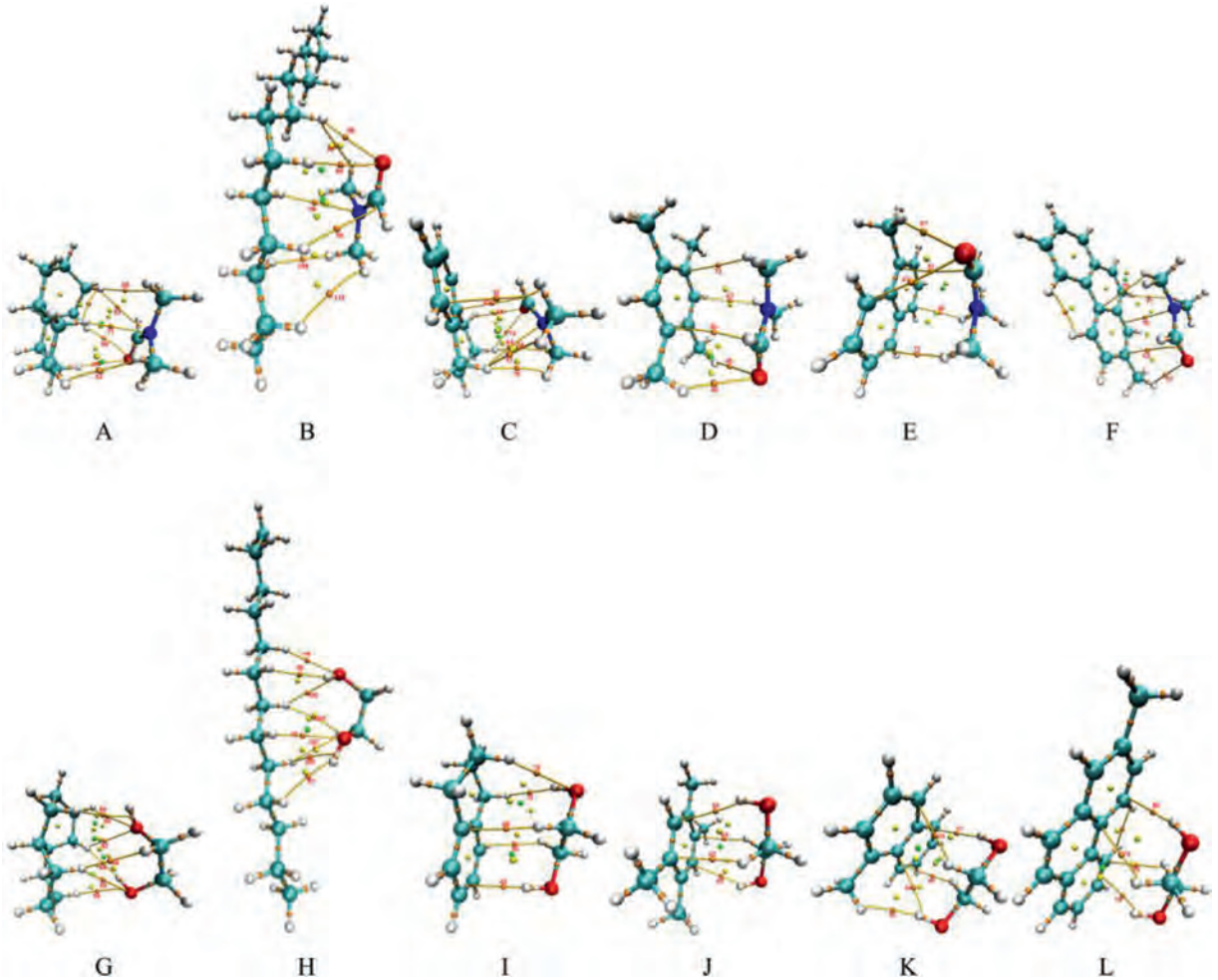


**Fig. 10.** BCPs distribution and bond paths of complexes in DMF and EG solvent systems, respectively: (A) DMF-decalin; (B) DMF-tridecane; (C) DMF-tetralin; (D) DMF-1,2,4,5-tetramethylbenzene; (E) DMF-1-methylnapthalene; (F) DMF-2-methylphenanthrene; (G) EG-decalin; (H) EG-tridecane; (I) EG-tetralin; (J) EG-1,2,4,5-tetramethylbenzene; (K) EG-1-methylnapthalene; (L) EG-2-methylphenanthrene.

value $\nabla^2\rho(r)$, total energy density $H(r)$, potential energy $V(r)$, kinetic energy $G(r)$, and $|V(r)|/G(r)$. In this work, all the investigated BCPs exhibit positive values of $\nabla^2\rho(r)$, $H(r)$, and $|V(r)|/G(r)$, which demonstrates the essence of non-covalent interactions [38,39] between the solvents and solute molecules. Additionally, $\rho(r)$, $\nabla^2\rho(r)$, and $H(r)$ can be used as quantitative indicators to characterize the strength of the bond. Koch and Popelier [40] indicated that the interaction can be ascribed to hydrogen bond if $\rho(r)$ ranges from 0.002 to 0.035 and $\nabla^2\rho(r)$ ranges from 0.024 to 0.139, while Rozas and Lipkowski [41,42] proposed that an interaction is identified as a weak hydrogen bond if the values of $\nabla^2\rho(r)$ and $H(r)$ are both positive. The BCPs and bond paths for the interactions between solvents and alkanes/aromatics are shown in Fig. 10. Based on these principles above, the numbers of BCPs that show weak hydrogen bonds between the solvents and solutes are as follows: 0 for {DMF + decalin} and {DMF + tetralin}; 1 for {DMF + tridecane}, {DMF + 1-methylnaphthalene}, and {DMF + 2-methylphenanthrene}; and 2 for {DMF + TMB}. For EG, there are 0 BCPs for {EG + decalin}, {EG + TMB}, {EG + 1-methylnaphthalene}, and {EG + 2-methylphenanthrene}; 1 for {EG + tetralin} and 2 for {EG + tridecane}. These BCPs are important supplements to the most stable configurations of the solvent-solute complexes. It is worth noting that the $\rho(r)$ values of the BCPs in all solvent-solute systems are very low due to the weak hydrogen bonds.

### 3.1.4. Extractive distillation performance of single solvent

A series of batch extractive distillation experiments were performed to verify the enrichment efficacy of single polar solvents on PAHs in FCC diesel and its extract. As presented in Fig. 11 and Fig. S4, EG and NFM exhibit similar separation performances regardless of whether FCC diesel or its extract is used as the feedstock. For the extractive distillation of FCC diesel, the recoveries of MAHs in the light fraction are 91.9% (mass) and 92.7% (mass) for EG and NFM, respectively, with corresponding $S$ of 26.7 and 28.0 (Fig. 12).

In contrast, for the extractive distillation of FCC diesel extract, the recoveries of MAHs in the light fraction are 96.0% (mass) and 88.0% (mass), with corresponding $S$ of 33.5 and 19.5, respectively. Interestingly, among these seven solvents except for EG, the $S$ for PAHs in the extractive distillation of FCC diesel is consistently higher than that of its extract. This appears to contradict the results from the previous solvent-free direct distillation experiments. It can be inferred that the higher alkane content in FCC diesel compared to its extract, coupled with the lower boiling points of some alkanes relative to aromatics, increases the relative volatility between PAHs and MAHs. Therefore, both EG and NFM are promising candidates for the main solvent, and EG is ultimately selected as the main solvent considering the differences in boiling points and the content of PAHs in the heavy fraction.

## 3.2. Optimization and evaluation of process route

The content of PAHs in the heavy fractions obtained from the extractive distillation of FCC diesel is lower than that of its extract, which can be attributed to their differences in chemical composition, as evidenced by the results of single solvent extractive distillation experiments. To maximize the added value of the products and simultaneously recover a portion of the PAHs, a secondary extractive distillation operation was carried out on the light fractions that result from the primary extractive distillation of FCC diesel. Accordingly, two separation processes for PAHs have been designed: The first process involves the enrichment of aromatic components in FCC diesel through solvent extraction, which is then used as the feedstock for extractive distillation. The resulting heavy fraction constitutes high-purity PAHs, while the light fraction can serve as a special solvent oil with low alkane content. Meanwhile, the second process entails the direct primary extractive distillation of FCC diesel, yielding the primary heavy fraction that contains PAHs and a primary light fraction subsequently subjected to secondary extractive distillation. Notably, the secondary heavy fraction can be recycled to the feed owing to its composition being similar to that of FCC diesel, whereas the secondary light fraction serves as a high-grade cracking feedstock enriched in alkanes and MAHs.

### 3.2.1. Determination of the solvent system and optimal condition

*3.2.1.1. Primary extractive distillation optimization.* As shown in Fig. 11, the recovery of PAHs in the light fraction obtained from the extractive distillation of FCC diesel extract using EG (43.0% (mass)) is significantly higher than that using NFM (27.4% (mass)). Therefore, NFM can be considered as an auxiliary agent to reduce the solubility of PAHs in the light fraction when EG is used as the main solvent, thereby enhancing the separation selectivity of

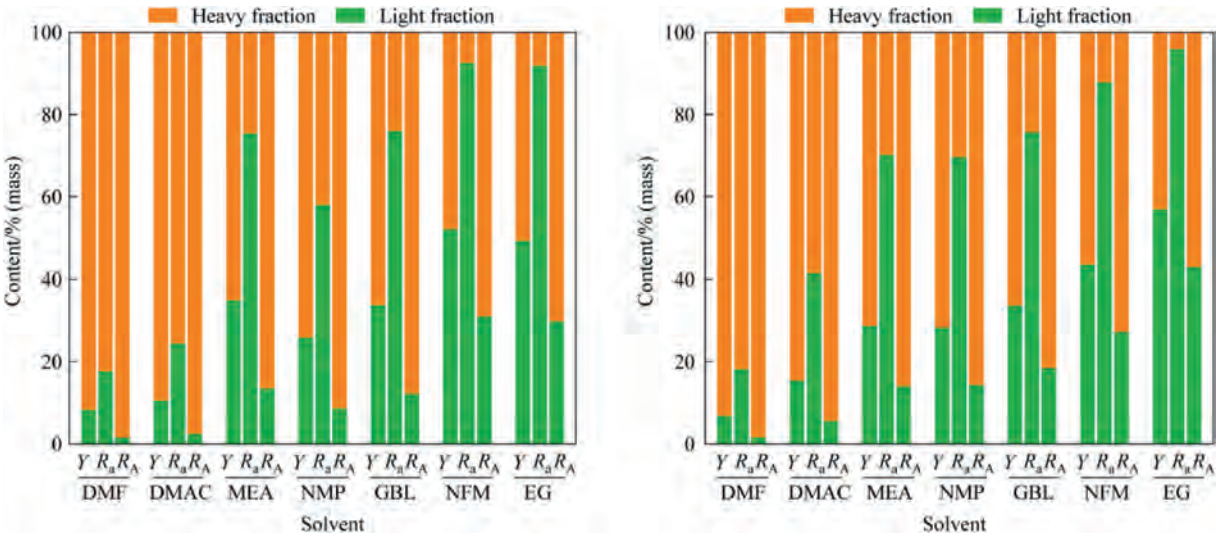


**Fig. 11.** Yield and recovery of fractions derived from primary extractive distillation of FCC diesel (left) and its extract (right) using diverse solvents.

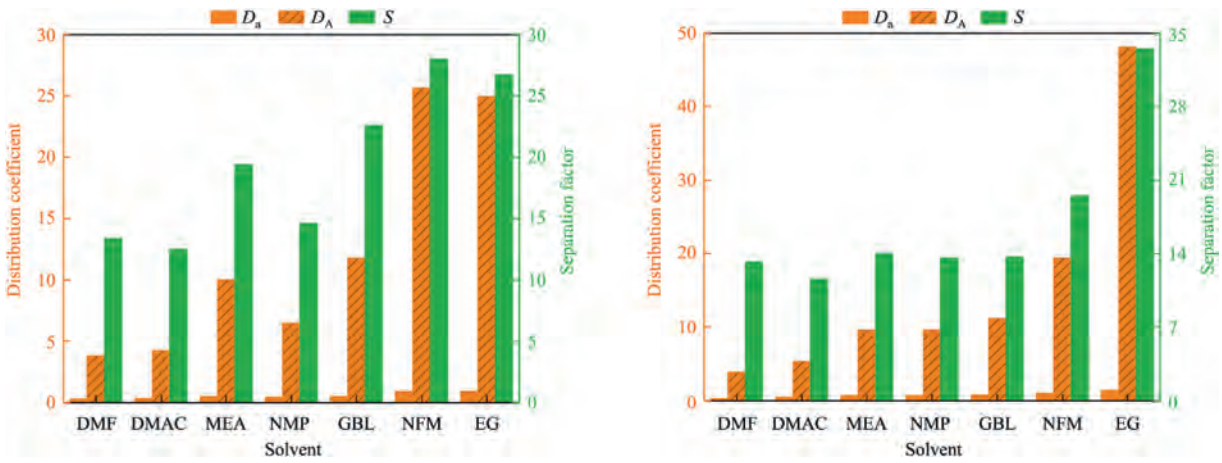


**Fig. 12.** Distribution coefficient and separation factor of primary extractive distillation of FCC diesel (left) and its extract (right) using diverse solvents.

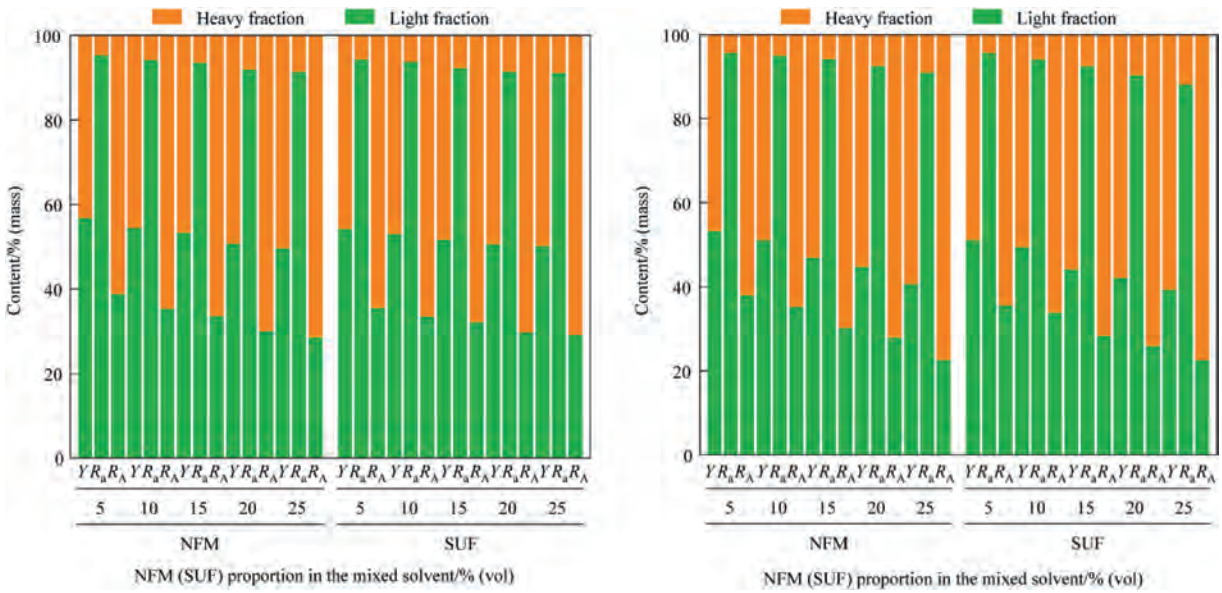


**Fig. 13.** Effect of co-solvent on the yield and recovery of fractions derived from primary extractive distillation of FCC diesel (left) and its extract (right).

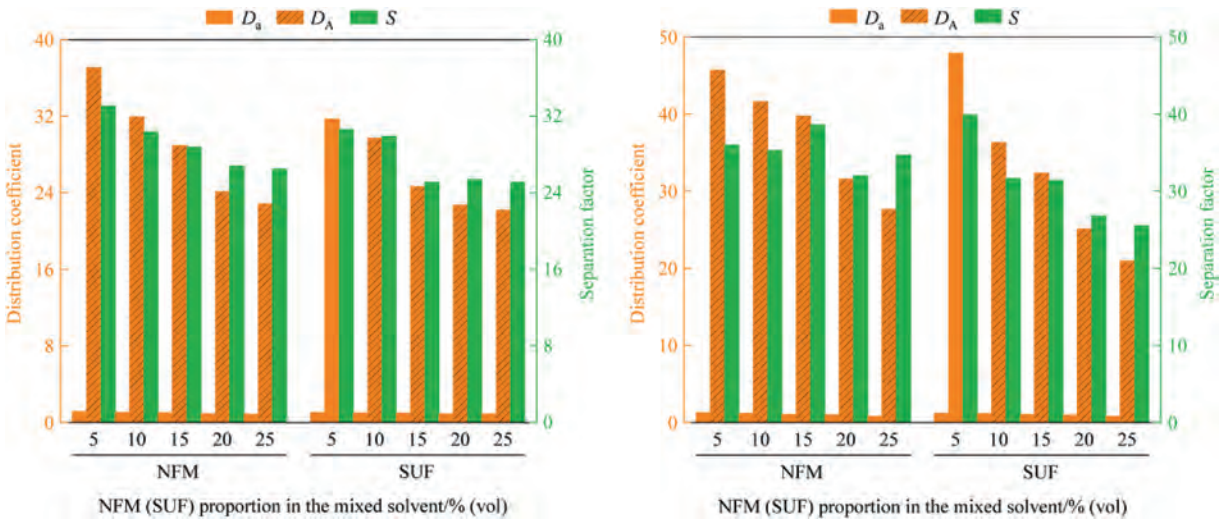


**Fig. 14.** Effect of co-solvent on the distribution coefficient and separation factor of primary extractive distillation of FCC diesel (left) and its extract (right).

PAHs. From this perspective, SUF, a solvent with higher polarity and boiling point than those of EG, is also a viable candidate.

As shown in Fig. 13, the yield of the light fraction decreases whereas that of the heavy fraction increases, while the recovery of PAHs in the light fraction decreases and the recovery in the heavy fraction rises. It can be seen from Fig. 14 that the separation selectivity of PAHs is reduced from 36.0 to 32.0 with the {EG + NFM} system and from 39.9 to 25.5 with the {EG + SUF} system when the volume ratio of the auxiliary agent is increased during the extractive distillation of FCC diesel extract. The experimental trends for the extractive distillation of FCC diesel using these two solvent systems are consistent with those observed for its extract, indicating that the addition of a strongly polar auxiliary agent with a high boiling point facilitates the retention of PAHs from the feedstock in the heavy fraction at the bottom of the column.

The previously discussed interaction energy patterns between solvents and PAHs/MAHs are aligned with this observation, where stronger intermolecular interaction energies with solvents are exhibited by PAHs due to their possession of more ESP extreme. It is noteworthy that NFM exhibits lower solubility for aromatics compared to SUF, as evidenced by the marginally decreased yield of the heavy fraction obtained from the extractive distillation using the {EG + NFM} solvent system compared to the {EG + SUF} solvent system. However, as presented in Fig. S5, the content of PAHs in the heavy fraction of the former is generally higher than that of the latter. Hence, NFM is selected as the auxiliary agent for both FCC diesel and its extract, with volume ratios of 5% and 15%, respectively.

As demonstrated in Fig. 15, for both feedstocks, an increase in the solvent/oil ratio results in an increase in the yield of the light fraction and a decrease in the yield of the heavy fraction. This trend suggests that an increased solvent dosage promotes the transfer of more volatile components into the light fraction during the extractive distillation, thereby allowing PAHs to dominate the heavy fraction. Taking into account both the economic viability and separation efficiency of the extractive distillation process, optimal solvent/oil ratios of 1.4 and 1.0 are screened for FCC diesel and its extract, respectively, corresponding to separation selectivities of 38.6 and 39.4 as shown in Fig. 16.

*3.2.1.2. Secondary extractive distillation optimization.* As indicated in Fig. 11 and Fig. S4, the light fraction derived from the extractive distillation of FCC diesel employing DMF contains a relatively high content (43.4% (mass)) of MAHs, while maintaining a limited yield of 8.4% (mass). On the one hand, this is attributed to the fact that DMF has the lowest boiling point among all the solvents investigated in this study, resulting in a lower final distillation temperature compared to other solvent systems. Additionally, the interaction energy between aromatics and DMF is significantly lower than that of other solvents, thereby suppressing the distillation of PAHs along with the solvent. On the other hand, DMF can be employed for the secondary extractive distillation of the primary light fraction to reduce the PAH content therein. Moreover, the recovery of PAHs in the light fraction when EG is used alone is lower than that of NFM. Therefore, in this section, the separation performance of {EG + DMF} solvent system on the primary light fraction was investigated, with EG serving as the main solvent and DMF as the auxiliary agent.

As shown in Fig. 17, the recovery of PAHs in the secondary light fraction decreases with increasing EG volume ratio, confirming that PAHs are retained in the secondary heavy fraction by EG (Fig. 18). As shown in Fig. S7, the chemical composition of the secondary heavy fraction closely matches that of FCC diesel when the volume ratio of EG reaches 40%, thus enabling its direct recycling back into the extraction process as a feedstock. However, as displayed in Fig. 19 and Fig. S8, the yield of the secondary heavy fraction significantly decreases as the solvent/oil ratio increases, causing the PAH content in the secondary light fraction to exceed 10% (mass). It can be found from Fig. 20 that a lower solvent/oil ratio restricts the migration of PAHs into the heavy fraction in the secondary extractive distillation process. In summary, the optimal solvent system for the secondary extractive distillation is determined to be {60% (vol) DMF +40% (vol) EG}, with a solvent/oil ratio of 0.5.

*3.2.2. Feasibility of extractive distillation*

The content and types of alkanes critically affect the separation efficiency of solvent extractive distillation of FCC diesel. Therefore, it is imperative to explore the generalizability of this method to various feedstocks. In this section, the primary extractive distillation separation efficiencies of FCC-2 and FCC-3 diesels and their corresponding extracts were investigated under the aforementioned optimal conditions (see Fig. 21).

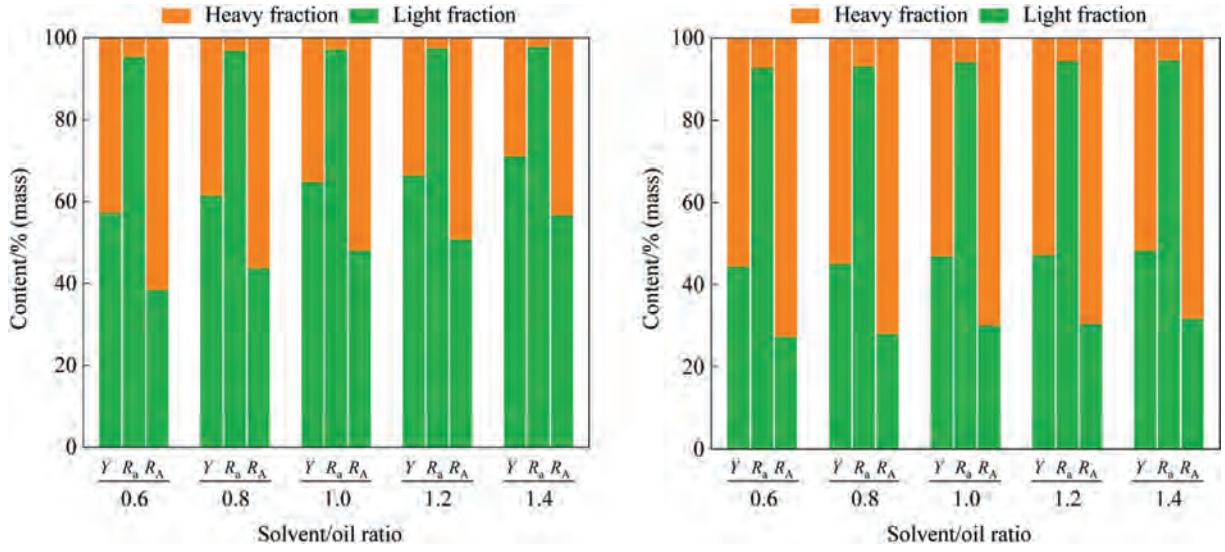


**Fig. 15.** Effect of solvent/oil ratio on the yield and recovery of fractions derived from primary extractive distillation of FCC diesel (left) and its extract (right).

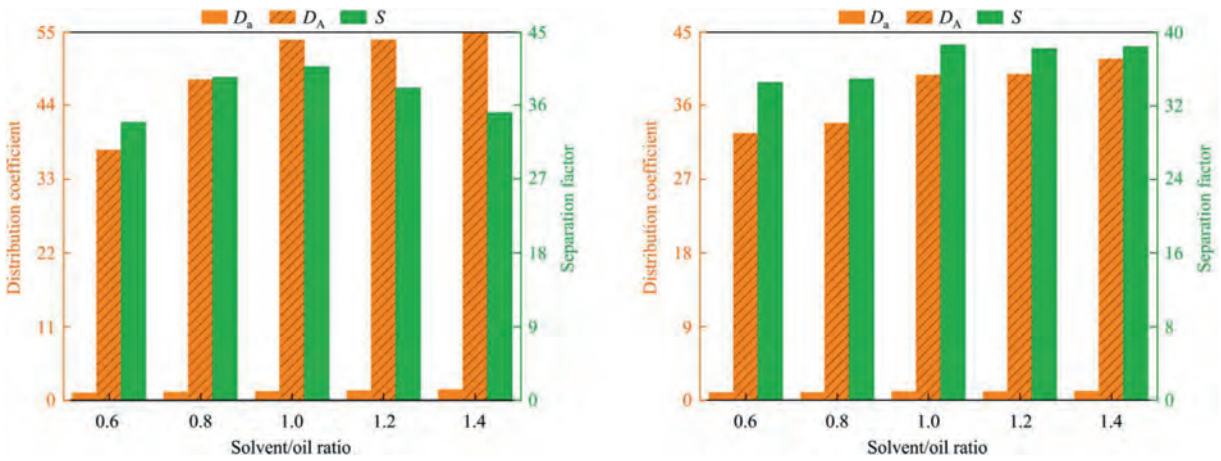


**Fig. 16.** Effect of solvent/oil ratio on the distribution coefficient and separation factor of primary extractive distillation of FCC diesel (left) and its extract (right).

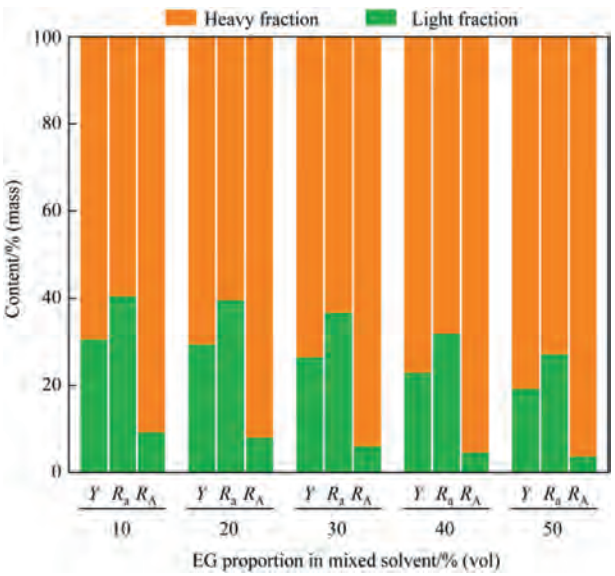


**Fig. 17.** Effect of EG on the yield and recovery of fractions derived from secondary extractive distillation of FCC diesel.

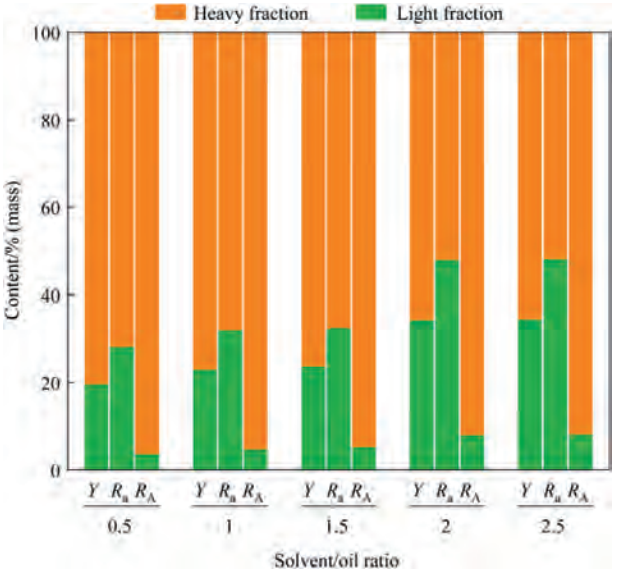


**Fig. 19.** Effect of solvent/oil ratio on the yield and recovery of fractions derived from secondary extractive distillation of FCC diesel.

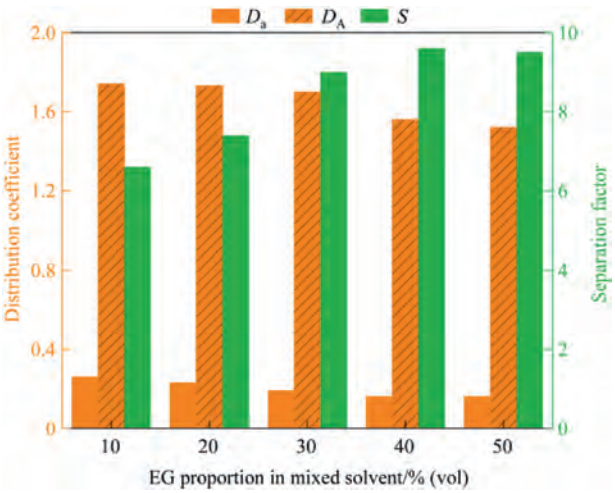


**Fig. 18.** Effect of EG on the distribution coefficient and separation factor of secondary extractive distillation of FCC diesel.

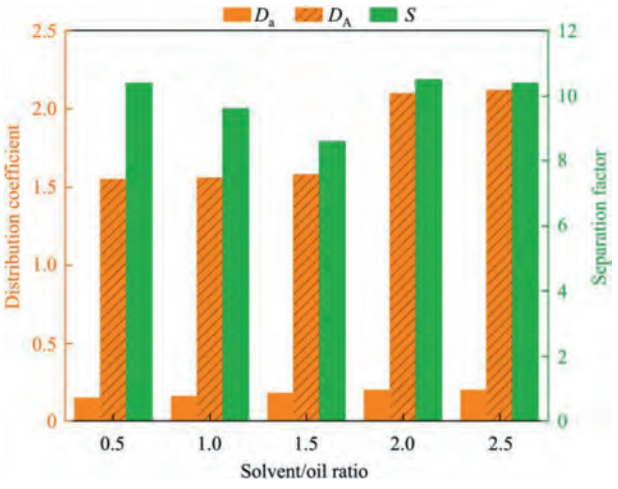


**Fig. 20.** Effect of solvent/oil ratio on the distribution coefficient and separation factor of secondary extractive distillation of FCC diesel.

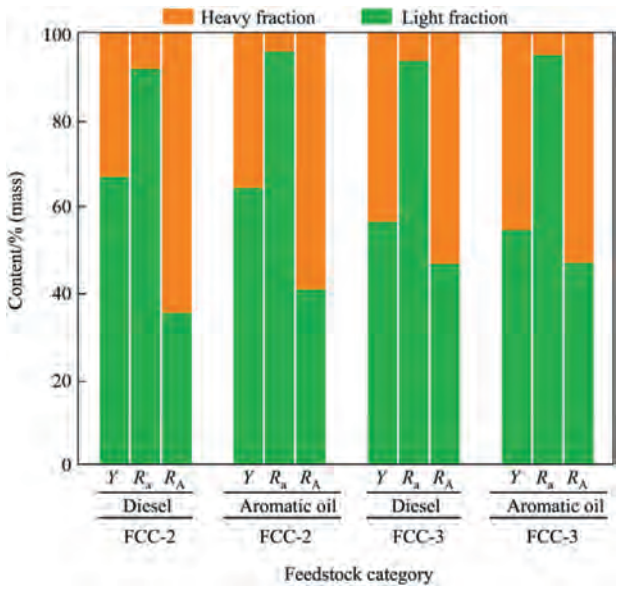


**Fig. 21.** Yield and recovery of fractions derived from primary extractive distillation of FCC-2/FCC-3 diesel (left) and their extracts (right) at optimal condition.

Notably, FCC-2 and FCC-3 diesels exhibit similar total aromatic mass contents (within ±5% (mass) variation) but significantly different MAH concentrations, with an approximately 20% difference observed between the two diesels. As indicated in Fig. 22 and Fig. S9, the separation selectivity of PAHs for the two FCC diesels and their corresponding extracts follows the order: FCC-2 ($S$ = 20.5) > FCC-3 ($S$ = 17.0), and FCC-2 diesel extract ($S$ = 34.3) > FCC-3 diesel extract ($S$ = 22.0). Obviously, higher alkane content in FCC-3 diesel is associated with lower $S$, while higher MAH content in FCC-2 diesel extract (41.1% (mass)) correlates with improved PAH separation compared to FCC-3 diesel(17.2% (mass)). The results suggest that the presence of alkanes is detrimental to enhancing the separation selectivity for PAHs, and feedstocks with higher MAHs content may exhibit better separation performance at the same experiment level.

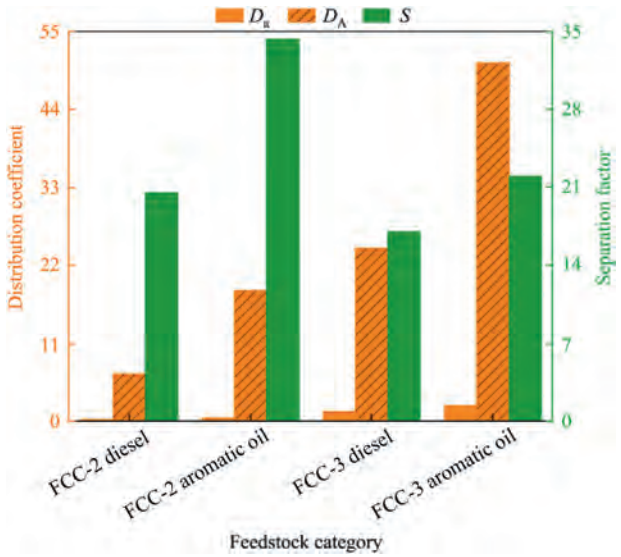


**Fig. 22.** Distribution coefficient and separation factor of primary extractive distillation of FCC-2/FCC-3 diesel (left) and their extracts (right) at optimal condition.

This potential separation strategy demonstrates favorable applicability for FCC diesel with varying PAH concentrations. Despite challenges in operational conditions and continuous operation, this study not only provides a precise solvent screening method for PAH extraction from FCC diesel but also confirms the transferability of calculated molecular property parameters to other systems. These findings facilitate industrial-scale directional separation of high-value products from complex hydrocarbon mixtures.

## 4. Conclusions

In this study, two processes were proposed for the separation of PAHs from FCC diesel via extractive distillation method coupled with solvent screening, and the generalizability of the method was subsequently verified using different types of FCC diesel. Firstly, MPI was identified as the optimal molecular polarity descriptor compared to other ones. The analysis of intermolecular interaction energies demonstrated that the energy difference range for alkane-aromatic interactions (−0.11 to −20.54 kJ·mol$^{-1}$) was significantly greater than that observed between MAHs and PAHs (−0.02 to −12.50 kJ·mol$^{-1}$). Among them, DMF and EG exhibited the highest interaction energy for all representative alkanes and aromatics, respectively. In addition, RDG and AIM analyses elucidated that the solvent-solute system was predominantly governed by weak vdW interactions, while ESP analysis further indicated that solvents with hydroxyl groups presented a higher propensity to form weak, non-classical hydrogen bonds with solutes. Furthermore, EG showed a high separation selectivity of up to 33.5 for PAHs in the extract derived from FCC diesel among the seven solvents used in the experiment. Moreover, the optimal solvent system for primary extractive distillation was determined to be a binary mixture of EG and NFM (co-solvent), with the volume fraction of NFM adjusted to 5% for FCC diesel and 15% for its extract, respectively. In contrast, the optimal solvent system for secondary extractive distillation consisted of 60% (vol) DMF and 40% (vol) EG (co-solvent). The two processes produce high purity PAH, with the PAH mass content reaching 95.0% for route 1 and 92.0% for route 2. Ultimately, experimental results from extractive distillation of two FCC diesels with distinct contents of MAH and PAH indicate that higher MAH concentrations in the feedstock significantly enhance the separation selectivity between MAH and PAH at the same experiment condition.

## CRediT Authorship Contribution Statement

Jun Li: Writing – original draft, Methodology, Investigation, Formal analysis, Data curation. Wanting Yu: Validation, Software, Formal analysis. Jinsen Gao: Writing – review & editing, Supervision, Project administration, Funding acquisition.

## Declaration of Competing Interest

The authors declare that they have no known competing financial interests or personal relationships that could have appeared to influence the work reported in this paper.

## Acknowledgements

This work was supported by the National Natural Science Foundation of China (22021004).

## Supplementary Material

Supplementary data to this article can be found online at https://doi.org/10.1016/j.cjche.2025.09.001.

## References


[1] J. Shin, Y. Oh, Y. Choi, J. Lee, J.K. Lee, Design of selective hydrocracking catalysts for BTX production from diesel-boiling-range polycyclic aromatic hydrocarbons, *Appl. Catal. A-Gen.* 547 (2017) 12–21.

[2] Q.H. Liu, G.X. Li, C.M. Gui, Z.G. Lei, Solvents evaluation for extraction of polycyclic aromatics from FCC diesel: experimental and computational thermodynamics, *Chem. Eng. Sci.* 264 (2022) 118205.

[3] W.K. Gao, C.L. Liu, Y.X. Chen, G.C. Guo, H. Wang, F.J. Yang, H. Jiang, Q.Y. Zhao, Q.M. Wu, B.X. Shen, H. Sun, Exploring ionic liquids for the extraction separation of aromatic hydrocarbons from diesel *via* multiple interaction analyses coupled with experimental evaluation, *Fuel* 368 (2024) 131634.

[4] F. Faisal, M.G. Rasul, M.I. Jahirul, A.A. Chowdhury, Waste plastics pyrolytic oil is a source of diesel fuel: a recent review on diesel engine performance, emissions, and combustion characteristics, *Sci. Total Environ.* 886 (2023) 163756.

[5] C. Hayichelaeh, K. Boonkerd, Utilization of palm oil as an alternative processing oil in carbon black-filled natural rubber compounds, *Ind. Crop. Prod.* 194 (2023) 116270.

[6] K. Sakamoto, K. Kawajiri, H. Hatori, K. Tahara, Impact of the manufacturing processes of aromatic-polymer-based carbon fiber on life cycle greenhouse gas emissions, *Sustainability* 14 (2022) 3541.

[7] Y.F. Qin, Z. Huang, K.X. Ma, L.P. Dong, J. Li, Q.C. Wang, Z.M. Xu, W.Q. Chen, Life cycle assessment of recycling high impact polystyrene and acrylonitrile butadiene styrene plastic from waste refrigerators, *J. Clean. Prod.* 435 (2024) 140294.

[8] R.K. Roy, T. Samanta, S. Saha, A. Ramesh, N.A. Begum, G. Ghosh, P. Dey, Aromatic *vs.* aliphatic linkers: impact on dye loading and stability in oligoglycerol-derived dendronized polymersomes, *Polym. Chem.* 16 (2025) 27–36.

[9] S.J. Lim, P. Fox, Effects of halogenated aromatics/aliphatics and nitrogen(*N*)-heterocyclic aromatics on estimating the persistence of future pharmaceutical compounds using a modified QSAR model, *Sci. Total Environ.* 470-471 (2014) 348–355.

[10] Y. Ma, L.X. Huang, Y.H. Tan, H.T. An, Q. Zhang, C.M. Xu, B.J. Shen, The regulating effect of zeolite types on catalytic aromatization of propane: the distributions of evaporable aromatics and non-evaporable polycyclic aromatics, *Fuel* 390 (2025) 134659.

[11] N.F. Nejad, E.K. Zand, A new approach to dearomatization of gasoline by ionic liquid and liquid-liquid extraction, *Petrol. Sci. Technol.* 29 (2011) 2372–2376.

[12] P. Navarro, I. De Dios-García, M. Larriba, N. Delgado-Mellado, M. Ayuso, D. Moreno, J. Palomar, J. García, F. Rodríguez, Dearomatization of pyrolysis gasoline by extractive distillation with 1-ethyl-3-methylimidazolium tricyanomethanide, *Fuel Process. Technol.* 195 (2019) 106156.

[13] M. Ayuso, P. Navarro, A.M. Palma, M. Larriba, N. Delgado-Mellado, J. García, F. Rodríguez, J.A.P. Coutinho, P.J. Carvalho, Separation of benzene from methylcycloalkanes by extractive distillation with cyano-based ionic liquids: experimental and CPA EoS modelling, *Sep. Purif. Technol.* 234 (2020) 116128.

[14] P. Navarro, M. Larriba, N. Delgado-Mellado, M. Ayuso, M. Romero, J. García, F. Rodríguez, Experimental screening towards developing ionic liquid-based extractive distillation in the dearomatization of refinery streams, *Sep. Purif. Technol.* 201 (2018) 268–275.

[15] S. Mukherjee, D. Sensharma, O.T. Qazvini, S. Dutta, L.K. Macreadie, S.K. Ghosh, R. Babarao, Advances in adsorptive separation of benzene and cyclohexane by metal-organic framework adsorbents, *Coord. Chem. Rev.* 437 (2021) 213852.

[16] T.F. Chen, W.X. Zhang, B. Li, W.B. Huang, C.H. Lin, Y. Wu, S.H. Chen, H.P. Ma, Adsorptive separation of aromatic compounds from alkanes by π-π interactions in a carbazole-based conjugated microporous polymer, *ACS Appl. Mater. Interfaces* 12 (2020) 56385–56392.

[17] G.B. Shan, H.Z. Liu, J.M. Xing, G.D. Zhang, K. Wang, Separation of polycyclic aromatic compounds from model gasoline by magnetic alumina sorbent based on π-complexation, *Ind. Eng. Chem. Res.* 43 (2004) 758–761.

[18] Y.M. Tu, H. Yu, W. He, Z.Y. Zhou, W. Liu, F. Zhang, Y.X. Qu, Z.Q. Ren, Application of ionic liquid-polymer gel membrane in toluene/*n*-heptane separation, *Sep. Purif. Technol.* 266 (2021) 118596.

[19] L. Aouinti, D. Roizard, M. Belbachir, PVC-activated carbon based matrices: a promising combination for pervaporation membranes useful for aromatic-alkane separations, *Sep. Purif. Technol.* 147 (2015) 51–61.

[20] C. Liu, D. Zhao, H.Y. Zhang, Y.G. Wang, H.C. Bai, Q. Liu, Cumene extraction separation from alkanes using DMSO: influence of the alkane structure, *Fluid Phase Equilib.* 550 (2021) 113236.

[21] L.Y. Zhang, X.D. Tang, J.J. Li, J. Yang, G.R. Dai, Extraction and separation of polycyclic aromatic hydrocarbons from catalytic cracking diesel, *J. Chem. Eng. Data* 68 (2023) 393–404.

[22] J. Mahmoudi, M.N. Lotfollahi, (Liquid+liquid) equilibria of (sulfolane+benzene+*n*-hexane), (*N*-formylmorpholine+benzene+*n*-hexane), and (sulfolane+*N*-formylmorpholine+benzene+*n*-hexane) at temperatures ranging from (298.15 to 318.15) K: experimental results and correlation, *J. Chem. Thermodyn.* 42 (2010) 466–471.

[23] M.D. Shi, W. Zeng, S.X. Song, M.T. Zhou, W. Wang, Measurement and correlation of ternary (liquid-liquid) equilibrium data for *n*-heptane + *p*-xylene + (furfural or dimethyl sulfoxide) system at 303.15 K and 323.15 K, *J. Chem. Thermodyn.* 149 (2020) 106175.

[24] S.H. Ali, H.M.S. Lababidi, S.Q. Merchant, M.A. Fahim, Extraction of aromatics from naphtha reformate using propylene carbonate, *Fluid Phase Equilib.* 214 (2003) 25–38.

[25] Z.H. Wang, W.Y. Fan, D.M. Xu, S.S. He, H.W. Huang, J. Gao, Y.L. Wang, Liquid-liquid-phase equilibrium for quaternary systems (*n*-decane + 1-tetradecene + 1-methylnaphthalene + sulfolane/dimethyl sulfoxide) for separation of 1-methylnaphthalene from FCC diesel, *J. Chem. Eng. Data* 66 (2021) 2803–2811.

[26] H.Y. Cheng, G.J. Zhang, Y.X. Zhang, Z. Song, Z.W. Qi, Solute structure effect on aromatics-alkanes extractive separation toward rational LCO upgrading, *Sep. Purif. Technol.* 310 (2023) 123213.

[27] X.L. Shi, Y.C. Song, Y.W. Wang, J. Feng, W.Y. Li, Precise regulation of weak intermolecular interaction forces and their application to high-purity aromatic monomer separation from direct coal liquefaction oil, *Sep. Purif. Technol.* 372 (2025) 133468.

[28] A.V. Marenich, C.J. Cramer, D.G. Truhlar, Universal solvation model based on solute electron density and on a continuum model of the solvent defined by the bulk dielectric constant and atomic surface tensions, *J. Phys. Chem. B* 113 (2009) 6378–6396.

[29] T. Lu, F.W. Chen, Multiwfn: a multifunctional wavefunction analyzer, *J. Comput. Chem.* 33 (2012) 580–592.

[30] Z.Y. Liu, T. Lu, Q.X. Chen, Intermolecular interaction characteristics of the all-carboatomic ring, cyclo[18]carbon: focusing on molecular adsorption and stacking, *Carbon* 171 (2021) 514–523.

[31] H. Fu, X.Y. Wang, H.N. Sang, Y.P. Hou, X.H. Chen, X. Feng, Dissolution behavior of microcrystalline cellulose in DBU-based deep eutectic solvents: insights from spectroscopic investigation and quantum chemical calculations, *J. Mol. Liq.* 299 (2020) 112140.

[32] J.S. Murray, P. Politzer, The electrostatic potential: an overview, *WIREs Comput. Mol. Sci.* 1 (2011) 153–163.

[33] R.F.W. Bader, M.T. Carroll, J.R. Cheeseman, C. Chang, Properties of atoms in molecules: atomic volumes, *J. Am. Chem. Soc.* 109 (1987) 7968–7979.

[34] H. Yu, X.J. Wu, C.Q. Geng, X.Y. Li, C.C. Du, Z.Y. Zhou, Z.Q. Ren, Highly selective extraction of aromatics from aliphatics by using metal chloride-based ionic liquids, *Chin. J. Chem. Eng.* 65 (2024) 222–229.

[35] E.R. Johnson, S. Keinan, P. Mori-Sánchez, J. Contreras-García, A.J. Cohen, W. Yang, Revealing noncovalent interactions, *J. Am. Chem. Soc.* 132 (2010) 6498–6506.

[36] M. Domagała, S.J. Grabowski, CH···N and CH···S hydrogen bonds influence of hybridization on their strength, *J. Phys. Chem. A* 109 (2005) 5683–5688.

[37] S. Emamian, T. Lu, H. Kruse, H. Emamian, Exploring nature and predicting strength of hydrogen bonds: a correlation analysis between atoms-in-molecules descriptors, binding energies, and energy components of symmetry-adapted perturbation theory, *J. Comput. Chem.* 40 (2019) 2868–2881.

[38] R.G.A. Bone, R.F.W. Bader, Identifying and analyzing intermolecular bonding interactions in van der Waals molecules, *J. Phys. Chem.* 100 (1996) 10892–10911.

[39] G.X. Zhan, B.X. Shen, H. Sun, X. Chen, Extractive distillation approach to the removal of dimethyl disulfide from methyl *tert*-butyl ether: combined computational solvent screening and experimental process investigation, *Ind. Eng. Chem. Res.* 57 (2018) 3348–3358.

[40] U. Koch, P.L.A. Popelier, Characterization of C-H-O hydrogen bonds on the basis of the charge density, *J. Phys. Chem.* 99 (1995) 9747–9754.

[41] I. Rozas, I. Alkorta, J. Elguero, Behavior of ylides containing N, O, and C atoms as hydrogen bond acceptors, *J. Am. Chem. Soc.* 122 (2000) 11154–11161.

[42] P. Lipkowski, S.J. Grabowski, T.L. Robinson, J. Leszczynski, Properties of the C-H···H dihydrogen bond: an ab initio and topological analysis, *J. Phys. Chem. A* 108 (2004) 10865–10872.